Volume 24, issue 9, September 2009 ISSN 0883-2927

ELSEVIER

Applied Geochemistry

JOURNAL OF THE INTERNATIONAL ASSOCIATION OF GEOCHEMISTRY

Continued on outside back cover

Applied Geochemistry 24 (2009) 1653–1665

Contents lists available at ScienceDirect

Applied Geochemistry

journal homepage: www.elsevier.com/locate/apgeochem

Size and elemental distributions of nano- to micro-particulates in the geochemically-stratified Great Salt Lake

Ximena Diaz [a,1], William P. Johnson [a,*], Diego Fernandez [a], David L. Naftz [a,b]

[a] Department of Geology and Geophysics, University of Utah, 135 S 1460 E Salt Lake City, UT 84112, USA
[b] US Geological Survey, 2329 West Orton Circle, Salt Lake City, UT 84119, USA

ARTICLE INFO

Article history:
Received 31 October 2008
Accepted 22 April 2009
Available online 3 May 2009

Editorial handling by Dr. R. Fuge

ABSTRACT

The characterization of trace elements in terms of their apportionment among dissolved, macromolecular, nano- and micro-particulate phases in the water column of the Great Salt Lake carries implications for the potential entry of toxins into the food web of the lake. Samples from the anoxic deep and oxic shallow brine layers of the lake were fractionated using asymmetric flow field-flow fractionation (AF4). The associated trace elements were measured via online collision cell inductively-coupled plasma mass spectrometry (CC-ICP-MS). Results showed that of the total (dissolved + particulate) trace element mass, the percent associated with particulates varied from negligible (e.g. Sb), to greater than 50% (e.g. Al, Fe, Pb). Elements such as Cu, Zn, Mn, Co, Au, Hg, and U were associated with nanoparticles, as well as being present as dissolved species. Particulate-associated trace elements were predominantly associated with particulates larger than 450 nm in size. Among the smaller nanoparticulates (<450 nm), some trace elements (Ni, Zn, Au and Pb) showed higher percent mass (associated with nanoparticles) in the 0.9–7.5 nm size range relative to the 10–250 nm size range. The apparent nanoparticle size distributions were similar between the two brine layers; whereas, important differences in elemental associations to nanoparticles were discerned between the two layers. Elements such as Zn, Cu, Pb and Mo showed increasing signal intensities from oxic shallow to anoxic deep brine, suggesting the formation of sulfide nanoparticles, although this may also reflect association with dissolved organic matter. Aluminum and Fe showed greatly increased concentration with depth and equivalent size distributions that differed from those of Zn, Cu, Pb and Mo. Other elements (e.g. Mn, Ni, and Co) showed no significant change in signal intensity with depth. Arsenic was associated with <2 nm nanoparticles, and showed no increase in concentration with depth, possibly indicating dissolved arsenite. Mercury was associated with <2 nm nanoparticles, and showed greatly increased concentration with depth, possibly indicating association with dissolved organic matter.

1. Introduction

Natural nanoparticles are ubiquitous in the environment; e.g. clay particles. In oxic aquatic environments, nanoparticles may also occur as carbonates, phosphates, oxides and oxyhydroxides; whereas, in anoxic environments nanoparticles can also occur as sulfides and related compounds (Drever, 2002). Nanoparticles also occur as organic matter (e.g. humic and fulvic acids) and biological nanoparticles (e.g. viruses) (Wigginton et al., 2007; McCarthy and Zachara, 1989).

Nanoparticle size distributions, elemental compositions, and surface characteristics are not static, but are continuously changing in the environment due to interactions with other environmental constituents and equilibration with varying geochemical conditions. Nanoparticles interact with dissolved inorganic and organic matter as well as with microbes (Wigginton et al., 2007; McCarthy and Zachara, 1989; Lead and Wilkinson, 2006). These interactions may cause the nanoparticles to aggregate and possibly form larger and less dense filamentous complexes than the original nanomaterial (Lead and Wilkinson, 2006; Buffle and Leppard, 1995; Jarvie and King, 2007). Size distributions may evolve in response to dissolution/precipitation reactions. For example, Fe oxyhydroxide nanoparticles may form by oxidation of aqueous Fe(II) to form stable Fe(III) oxyhydroxide nanoparticles (with sizes ranging from 25 nm to 1000 nm) at near neutral pH (Gilbert et al., 2007).

Commonly used nanoparticle characterization techniques lack the ability to fractionate and characterize the nanoparticles efficiently (Baalousha and Lead, 2007a,b; Baalousha et al., 2006b) and suffer from individual limitations and artifacts, necessitating the application of multiple methods to characterize nanoparticles in natural aquatic media (Lead and Wilkinson, 2006). Flow-field

* Corresponding author. Tel.: +1 801 581 5033; fax: +1 801 581 7065.
E-mail address: william.johnson@utah.edu (W.P. Johnson).
[1] Present address: Department of Extractive Metallurgy, Escuela Politécnica Nacional, Quito – Ecuador.

0883-2927/$ - see front matter © 2009 Elsevier Ltd. All rights reserved.
doi:10.1016/j.apgeochem.2009.04.031

flow fractionation (FlFFF) is a low invasive method that uses hydrodynamic principles to separate particles by size. Nanoparticle separation using the FlFFF occurs in a thin rectangular channel (Giddings, 1985, 1993; Beckett and Hart, 1993). Use of a trapezoidal channel in so-called asymmetric flow-field flow fractionation (AF4) reduces sample dilution relative to symmetric channels (Prestel et al., 2005; Wahlund, 2000), and provides exceptional nanoparticle size resolution (Giddings, 1985, 1993; Beckett and Hart, 1993; Baalousha and Lead, 2007b). Buffle and Leppard (1995), Lyvén et al. (2003), and Lead and Wilkinson (2006) described important limitations in the fractionation of colloids from natural waters by FFF, including: aggregate modification during pretreatment and analysis via dilution, focusing, and accumulation near the membrane, as well as sample loss to the membrane.

The utility of combining sensitive elemental analysis (ICP-MS) to low-invasive fractionation by FFF was first demonstrated nearly two decades ago (e.g. Beckett, 1991; Taylor et al., 1992; Murphy et al., 1993), and has since then been implemented in widespread studies (Ranville et al., 1999; Hassellöv et al., 1999; Amarasiriwardena et al., 2001; Al-Ammar et al., 2001; Siripinyanond et al., 2002; Schmitt et al., 2002; Contado et al., 2003; Lyvén et al., 2003; Siripinyanond et al., 2005; Prestel et al., 2006; Bolea et al., 2006; Suteerapataranon et al., 2006; Ranville et al., 2007). AF4 coupled with inductively-coupled plasma mass spectrometry (ICP-MS) allows on-line determination of nanoparticle size distribution and elemental composition simultaneously (Baalousha et al., 2006a; Hassellöv et al., 1999; Lyvén et al., 2003; Stolpe et al., 2005). AF4-ICP-MS has been used successfully as well to examine the interaction of natural nanoparticles with trace elements (Baalousha et al., 2006a; Lyvén et al., 2003; Siripinyanond et al., 2002). Few publications are available for similar investigations in saline waters (Stolpe and Hassellöv, 2007). Colloidal particles in seawaters, particularly in estuaries, have typically been characterized chemically prior to fractionation via ultrafiltration techniques (Singhal et al., 2006; Kraepiel et al., 1997; Sañudo-Wilhelmy et al., 1996; Wells et al., 1998, 2000; Wen et al., 1997; Dai and Martin, 1995).

The Great Salt Lake (GSL) is a useful field laboratory in which to test methods for analysis of nanoparticles. Being a hypersaline terminal lake, the GSL has high concentrations of dissolved solids and it is supersaturated with respect to many phases containing major and trace elements (Stephens, 1990). The flow of higher density water (1160 kg m^{-3}) from the north arm to the less dense south arm (1100 kg m^{-3}), yields a persistent layered system (Lin, 1976), with an oxic brine upper layer and an anoxic brine deeper layer, yielding strongly contrasting geochemical conditions over a 9 m vertical distance (Tayler et al., 1980; Stephens, 1990; Gwynn, 2002). Temporal trends in the measured physical and chemical parameters in both brines demonstrate this strong redox stratification (as well as pH, conductivity, and temperature) in the lake (Figs. 1 and 2). The GSL hosts a large avian population that is potentially affected by trace metals and metalloids such as Se, As and Hg (Aldrich and Paul, 2002; Naftz et al., 2008), and natural nanoparticulates may act as a gateway for introducing trace elements into the food chain of the lake (Hillwalker, 2004; Dobbeleir et al., 1980). Laboratory experiments have proven that mineral nanoparticles may be directly ingested by mixotrophic phytoplankton (Hochella et al., 2008), which constitute the base of the GSL food chain (Wurstbaugh, 1992). The near-surface atomic structure, crystal shape and surface topography of natural nanoparticles is expected to render them more reactive to processes such adsorption and complexation of trace elements (Hochella et al., 2008; Wigginton et al., 2007) which also influences the behavior of these contaminants in natural waters (Morrison and Benoit, 2001; Baalousha and Lead, 2007a,b; Hochella et al., 2008; Wigginton et al., 2007; Lyvén et al., 2003). This work examines the size distribution and elemental composition of nanoparticles from oxic and anoxic samples in the GSL, with the working hypothesis being that the size and elemental distributions differ strongly among the oxic and anoxic layers of the GSL.

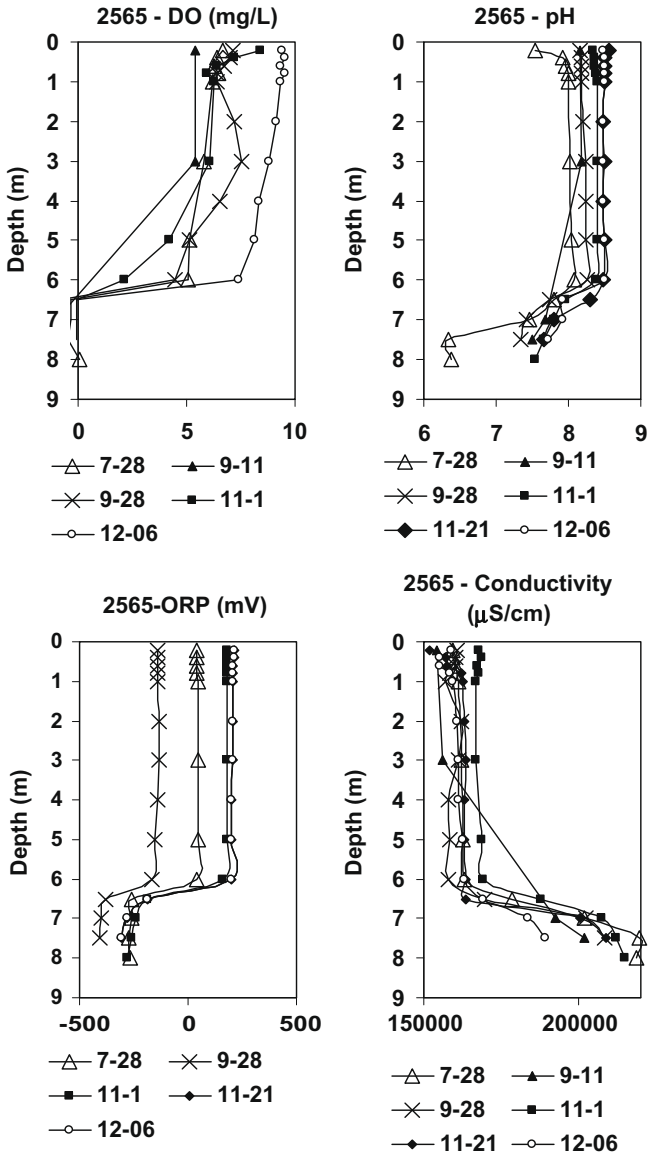

Fig. 1. Selected results for physical and chemical characteristics of the south arm of the Great Salt Lake. Site 2565 represents the location of sample collection and measurement, as shown in Fig. 3. For data collection details please see the Supplementary material.

2. Materials and methods

2.1. Location and sampling

Water samples for particulate analysis were taken at four stations (2267, 2565, 2767 and 3510) across the GSL (Fig. 3). Samples (250 mL) were collected monthly from each location using a peristaltic pump with acid-rinsed C-flex tubing (Cole-Parmer's Masterflex, Vernon Hills, IL) at different depths ranging from 0.2 to 8.0 m below the lake surface. Unfractionated samples were acidified *in-situ* (trace metal grade HNO_3, 2 mL, 7.7 N). Before acidification, one aliquot was filtered *in-situ* (450 nm cut-off) to allow comparison of raw acidified (RA) and filtered acidified (FA) trace element concentrations. Samples to be used in fractionation by AF4 were

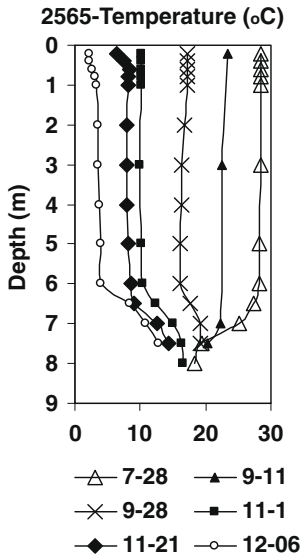

Fig. 2. Temperature profiles during the period of study. Site 2565 represents the location of sample collection and measurement, as shown in Fig. 3. For data collection details please see the Supplementary material.

chilled (without filtration and acidification), and were analyzed for size and elemental distribution within 3 days following collection, as suggested by Buffle and Leeuwen (1992, 1993). Raw (unfiltered, unacidified, RU) samples for total organic C (TOC) analysis were collected in acid-rinsed amber glass 250-mL bottles. All samples were stored in the laboratory at 4 °C.

TOC analysis were carried out at the University of Utah Center for Water, Ecosystems, and Climate Sciences (CWECS) laboratory facility using a TOC-5000 (Shimadzu, Columbia, MD) where water samples were analyzed sequentially for total C (TC) and inorganic C (IC), the TOC being the difference between TC and IC. In both analyses, the C contained in the sample was converted to CO_2 and analyzed by an infrared CO_2 analyzer. For TC analyses, the sample was heated at 680°C, while for the IC, the sample was acidified with H_3PO_4 (25%). QC samples included a duplicate, spike, check standard, spike standard and a blank.

Selected raw unacidified (RU) samples from deep and shallow brines were analyzed by scanning electron microscope (SEM) – energy dispersive X-ray spectroscopy (EDX) using a Hitachi S-3000N at the Material Science Department (University of Utah). RU shallow samples were filtered using a 0.22 μm pore size GTTP filter (Isopore™ membrane, polycarbonate, hydrophilic, 25 mm in diameter from Millipore), washed with milli-Q water and left to dry in a glove bag under a N_2 atmosphere. RU deep brine samples were centrifuged at 10,000 RPM for 50 min. The pellet was freeze-dried and then suspended with O_2-free milli-Q water in a glove bag under a N_2 atmosphere. The suspension was centrifuged at 10,000 RPM for 50 min. The pellet was left to dry under a N_2 atmosphere in a glove bag.

2.2. Fractionation

Suspended solids from 7 RU samples collected at two different locations (sites 2267 and 3510 – Fig. 3), and 3–4 different depths (spanning the deep and shallow brine layers), were fractionated into different sizes using asymmetric flow field-flow fractionation (AF4) (Postnova Analytics, Landsberg, Germany). Principles, techniques and operation procedures for the flow-field flow fractionation (FIFFF) and AF4 are described elsewhere (Giddings, 1985, 1993; Beckett and Hart, 1993; Prestel et al., 2005; Wahlund, 2000). A 10 KDa regenerated cellulose membrane was used in the AF4 channel, and was calibrated using standard nanoparticles. AF4 analysis was performed for two size ranges, 10–250 nm and 0.9–7.5 nm. This range separation was necessitated by the use of surfactant in the carrier solution for nano-particulates >10 nm, as described below. Colloidal Au and fluorescent latex beads with known sizes (10, 98 and 200 nm) were used to optimize operating conditions for the nanoparticle size range between 10 and 250 nm (Table 1, Fig. S2 in Supplementary material), which involved three cross-flows during elution to improve the particle separation and the intensity of the UV signal. Polystyrene sulfonate standards (PSS) with known molecular weights (8 KDa, 18 KDa, 35 KDa and 100 KDa) were used to optimize operating conditions for nanoparticles between 0.9 and 7.5 nm in the AF4 (Table 2, Fig. S3 in Supplementary material). A 4-step program for cross-flow in the AF4 was used during elution to improve particle separation and signal intensity.

To convert apparent molecular weight from the <7.5 nm nanoparticles to hydrodynamic diameter, the following expression from Prestel et al. (2005) was used: $\log d_h = 0.6685 \log MW - 2.6517$, where d_h is the hydrodynamic diameter (in nm) and MW is the molecular weight (in Da). More details of the AF4 calibration are presented in the Supplementary material.

Combining a collision cell (CC) with ICP-MS has been proven to successfully remove polyatomic interferences that may hamper elemental analyses (e.g. $^{40}Ar^{40}Ar$; $^{40}Ar^{35}Cl$ and $^{38}Ar^{37}Cl$) (Chen et al., 2007). To determine the trace element distribution in fractionated particulates, the AF4 was coupled with a CC-ICP-MS Agilent 7500ce (Agilent Technologies, Inc., Santa Clara, CA, USA). The CC-ICP-MS was used in a continuous mode (Table S1 in Supplementary material) and was calibrated using Cs added to the AF4 carrier solution (1 μg/L) as an internal standard. Adding internal standard to the carrier (rather than the sample) avoids discrepancies due to variations in solution flow to the detector during fractionation. To increase the sensitivity of trace elements such as Se and As, methanol was added to the carrier solution (3% v:v). A total of 17 elements (Al, S, Mn, Fe, As, Co, Ni, Cu, Zn, Mo, Se, Sb, Au, Hg, Pb, U, Cs) were measured online via CC-ICP-MS. Two types of carriers suggested in the literature were used (Moon, 1995; Barman and Moon, 2000; Cardot et al., 2001; Jeon et al., 1997; Cho et al., 2006; Reschiglian et al., 2000; Bolea et al., 2006; Ranville et al., 2007; Prestel et al., 2006; Lyvén et al., 2003; Koliadima and Karaiskakis, 1994). The carrier was 0.01 M NaCl for nanoparticle sizes ranging from approximately 0.9 to 5 nm (and macromolecule standards ranging from 8 KDa to 100 KDa). The carrier was 0.01% FL-70 surfactant for nanoparticle sizes ranging between 10 to 250 nm. The pH in the carriers was regulated to a value of 8.2 ± 0.3 using NaOH 0.1 N. Carrier pH was adjusted to the pH of the brine to avoid precipitation or other undesired reactions. The ionic strength was 0.01 M for the NaCl carrier, and was approximately 10^{-3} M for the FL-70 carrier (Koliadima and Karaiskakis, 1994), which is much lower than that of the brine samples in order to avoid precipitation in the cones during the continuous CC-ICP-MS analyses. Carriers used for fractionation must be compatible with the membrane and must minimize changes in sample aggregation state. Sodium chloride is the major dissolved component in the GSL. The NaCl carrier produced excellent macromolecule fractionation as demonstrated by the polystyrene sulfonate standards (PSS) (Fig. S3 in Supplementary material); however, this carrier produced poor fractograms for the 10 nm-colloidal Au and the 98 and 200 nm carboxylate-modified polystyrene microspheres, for which the surfactant FL-70 (Fig. S2 in Supplementary material) was used, as with with previous studies (Moon, 1995; Barman and Moon, 2000; Cardot et al., 2001; Jeon et al., 1997; Cho et al., 2006; Reschiglian et al., 2000; Koliadima and Karaiskakis, 1994). FL-70 is a mixture of anionic and nonionic surfactants that enhance the dispersion of particles, preventing aggregation (Moon, 1995).

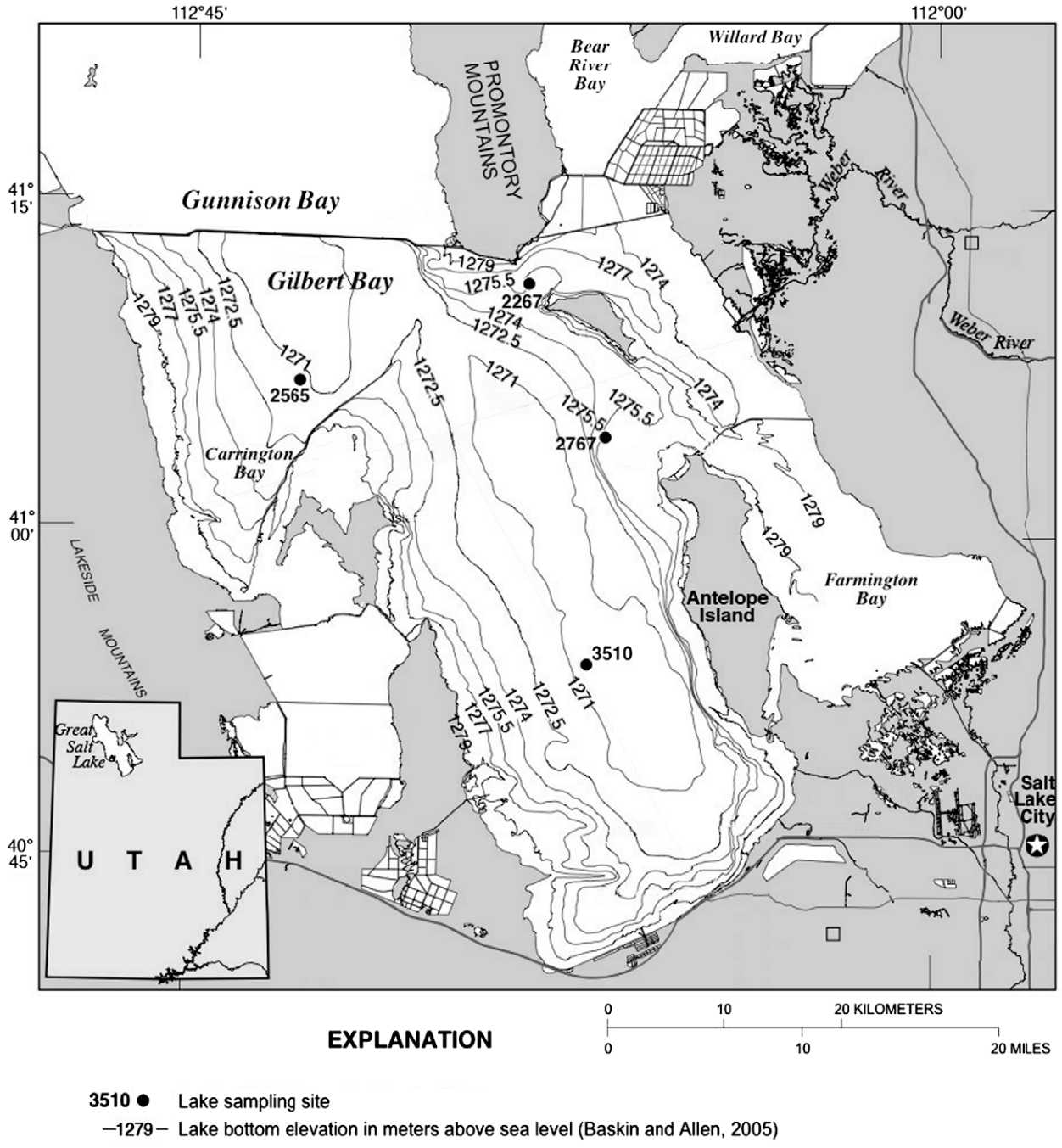

Fig. 3. Sampling locations (shown as circles) in the south arm of the Great Salt Lake. Map courtesy of the USGS.

The optimal concentration of carrier was determined on the basis of highest particle peak fractogram signals in preliminary tests.

To evaluate the potential for matrix interference during fractionation, a synthetic GSL solution matching the major ion content of the GSL water was examined in the AF4-CC-ICP-MS for all fractionation conditions. To identify interferences in blank samples, Milli-Q water was also examined under all fractionation conditions. Details regarding the synthetic solution and Milli-Q water AF4 results are presented in the Supplementary material.

The concentration of trace elements in particulates fractionated via AF4-CC-ICP-MS was determined by integrating the area under the fractogram for each element. The corresponding GSL synthetic signal was used as baseline (Figs. S4b and S5b in Supplementary material). The internal standard (Cs) signal in counts per second (cps) (corresponding to 1 μg/L) was used to convert the integrated area for all elements to their respective masses, according to the following equation:

$$Mass_i(\mu g) = \frac{Flow_{ICPMS}(mL/\min) * Area_i(counts)}{6 * 10^4 * RF_{Cs}\left(\frac{cps_{Cs}}{1\mu g/L}\right) * f_i\left(\frac{cps_i}{cps_{Cs}}\right)}$$

where $Flow_{ICPMS}$ is the flow entering the ICP-MS (in mL/min); $Area_i$ is the integrated area calculated for each element (in counts); RF_{Cs} is the *Cs* response factor (cps *Cs*/1 μg/L); and, f_i is the ionization efficiency correction factor for each element according to the Saha-Eggert equation (Taylor, 2001). The mass determined by integration was converted in concentration dividing the result obtained for the AF4 injection volume (300 μL). The AF4 carriers were spiked

Table 1
AF4 normal mode operation conditions (10–250 nm size range).

Operation conditions				
Volume loop (μL)	100–300			
UV λ (nm)	254			
Carrier	0.01% FL-70 + 3% MeOH + 1 ppb Cs			
Membrane	10 K Da regenerated cellulose			
	Injection	Elution 1	Elution 2	Elution 3
Injection volume (μL)	50–300			
Channel flow (mL/min)	0.1	4	3.7	3.5
Focus flow (mL/min)	3.9			
Cross flow (mL/min)	1	1	0.7	0.5
Slot flow (mL/min)	2.7	2.7	2.7	2.7
Detector flow (mL/min)	0.3	0.3	0.3	0.3
Pressure (bar)	3.7	3.4	3.4	3.4
Time (min)	5	5	4	5
Transition time (min)	1			
Rinsing time (min)	5			

with 10 ppb of each of the 17 elements analyzed by CC-ICP-MS to determine the change in the intensity ratio for each element relative to Cs compared to ionization efficiency correction factors for each element. Results showed good agreement for all of the elements analyzed, showing less than 30% difference between both values, indicating that Cs was a sufficiently sensitive internal standard to achieve accurate results.

3. Results

3.1. Trace element distribution among particulate sizes and lake layers

The fraction of total (dissolved + particulate) trace elements associated with particulates >450 nm was calculated as the difference between the raw acidified (RA) and the filtered acidified (FA) samples, divided by the raw acidified (RA). These values (expressed as percentages, Fig. 4) were arithmetically averaged among 86 shallow brine samples and 46 deep brine samples taken from four locations (Fig. 3) across the south arm of the GSL. Averaging the concentrations was justified by their consistency over space and time, as demonstrated by the small error bars associated with these averages (Fig. S1 in Supplementary material).

The concentration of >450 nm-associated trace elements was higher in the anoxic deep brine layer relative to the oxic shallow brine layer for the majority of the elements such as Al, Fe, Cu, Mo, Pb, Se, Ba, Ni, Mn, V, Zn, U and Co (Fig. 4). Major elements such as Na, Mg, S, Ca and K and trace elements such as Ti, Li, As, and Sb showed insignificant concentrations in the particulate phase relative to the dissolved phase (Fig. 4).

Table 2
AF4 normal mode operation conditions (0.9–7.5 nm size range).

Operation conditions					
Volume loop (mL)	100–300				
UV λ (nm)	254				
Carrier	0.01M NaCl + 3% MeOH + 1 ppb Cs				
Membrane	10 KDa regenerated cellulose				
	Injection	Elution 1	Elution 2	Elution 3	Elution 4
Injection volume (mL)	20–300				
Channel flow (mL/min)	0.1	4	3	2	1.5
Focus flow (mL/min)	3.9				
Cross flow (mL/min)	3	3	2	1	0.5
Slot flow (mL/min)	0.7	0.7	0.7	0.7	0.7
Detector flow (mL/min)	0.3	0.3	0.3	0.3	0.3
Pressure (bar)	2	2	2	2	2
Time (min)	5	4	3	3	5
Transition time (min)	1				
Rinsing time (min)	10				

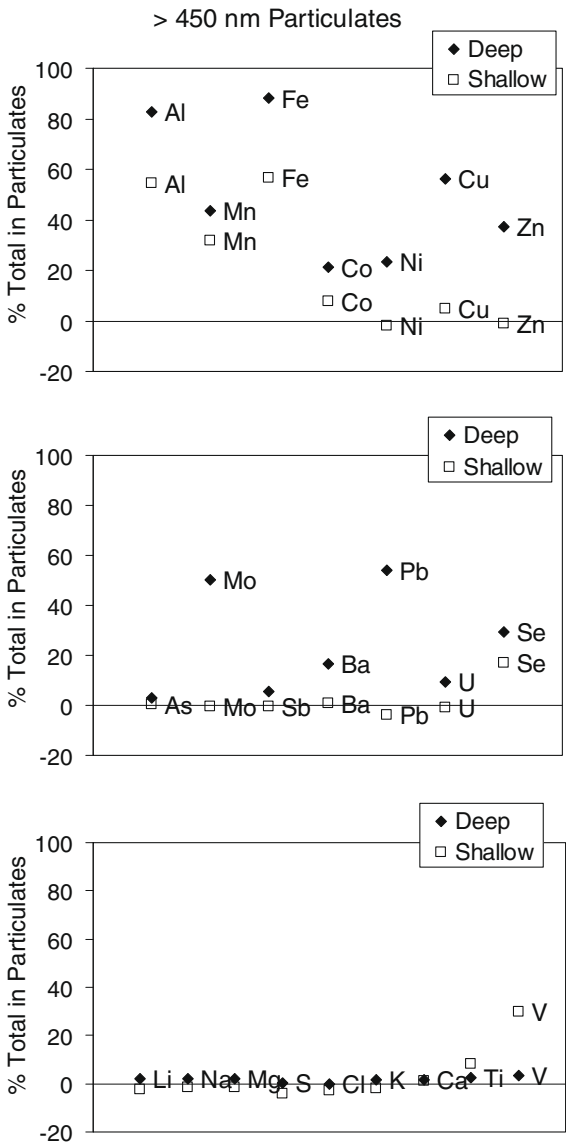

Fig. 4. Percentage of total (dissolved plus particulate) associated with >450 nm particulates. The percentage is calculated as the difference between the raw acidified (RA) and the filtered acidified (FA) divided by the RA and multiplied by 100.

Fractograms obtained under AF4 conditions for the 10–250 nm particulate size range showed trace elements associated with nanoparticles in the size range between 10 and 50 nm (Figs. 5 and 6), including Cu, Al, Mn, Fe, Zn, Pb, Ni U, Co, and Au. These elemental associations with the 10–50 nm size range were observed in both the shallow and the deep brine layers (Figs. 5 and 6). For the majority of the elements associated with nanoparticulates in the 10–50 nm size range, the concentration (signal intensity) of trace elements was higher in the anoxic deep brine layer relative to the oxic shallow brine layer (Figs. 5 and 6).

Notably, nanoparticles containing the monitored elements were not observed in the 50–250 nm size range with the exception of Zn (Fig. 5). Zinc is the only element that showed a peak associated with particulates in the size range from 110 nm to 200 nm in the deep brine sample (Fig. 5). No trace elements were detected in particulates between 50–250 nm in the shallow brine samples (Figs. 5 and 6). The lack of elemental signals in the rinse peak (Figs. 5 and 6) may indicate a lack of particles in the 250–450 nm size range as well, since these larger particles would likely have been released

during rinsing of the system (relaxation of the cross flow, as explained in the Supplementary material). In contrast, a significant signal was observed during rinsing under conditions for fractionation of nanoparticles in the 0.9–7.5 nm size range (Figs. 7 and 8), which corroborates the detection of nanoparticles in the void volume for the 10–50 nm size range. However, it should be noted that the rinse peak may also represent nanoparticles that were associated with the membrane under the elution conditions due to their surface chemistry and shape (not necessarily larger). In contrast to the rinse peak, the void peak may represent nanoparticulates too small to be attenuated by the applied cross flow, and particles that were not correctly focused. In the present case, the void peak observed in the fractograms for the 10–250 nm size range (Figs. 5 and 6) may indicate the presence of nanoparticles in the <10 nm size range, as was confirmed via fractionation under conditions corresponding to the 0.9–7.5 nm size range (Figs. 7 and 8).

Trace elements such as Mn, Pb, Zn, Cu, U, Ni and Co were associated with nanoparticles in the 1–2 nm size range, as well as the 5–7.5 nm size range. These nanoparticle size fractions and elemental associations with Mn, Pb, Zn, Cu, U, Ni and Co were observed in both the shallow and deep brine samples (Figs. 7 and 8), whereas the signal intensities were much greater for these elements (except Ni) in the deep brine layer (Fig. 7). Fig. 7 shows a continuum in signal intensities for these elements, increasing with increasing depth and degree of O_2 depletion. In the oxic shallow brine samples, As and Mo were associated only with nanoparticles in the 1–2 nm size range; whereas, in the anoxic deep brine layer samples these elements were associated with nanoparticles in the 1–2 nm size and in the 5–7.5 nm size range (Figs. 7 and 8). Aluminum showed a peak only in the 5–7.5 nm size range (not in the 1–2 nm size range) with this peak being somewhat larger in the deep brine samples relative to the shallow brine samples (Figs. 7 and 8). Mercury was significant in the 1–2 nm size in the anoxic deep brine sample, but was not present in the shallow brine samples. No void peak was observed under conditions corresponding to the 0.9–7.5 nm size range, suggesting that all monitored elements were associated with nanoparticles (or macromolecules) in the size range 0.9 nm and larger (Figs. 7 and 8). The signal intensities from the deep versus shallow brine layer samples from site 3510 showed major differences (Figs. 5 and 7). In contrast, the signal intensities for samples from different depths at site 2267, where no deep brine layer was present, showed no significant differences (Figs. 6 and 8). It should be noted that the raw signal intensities in Figs. 5–8

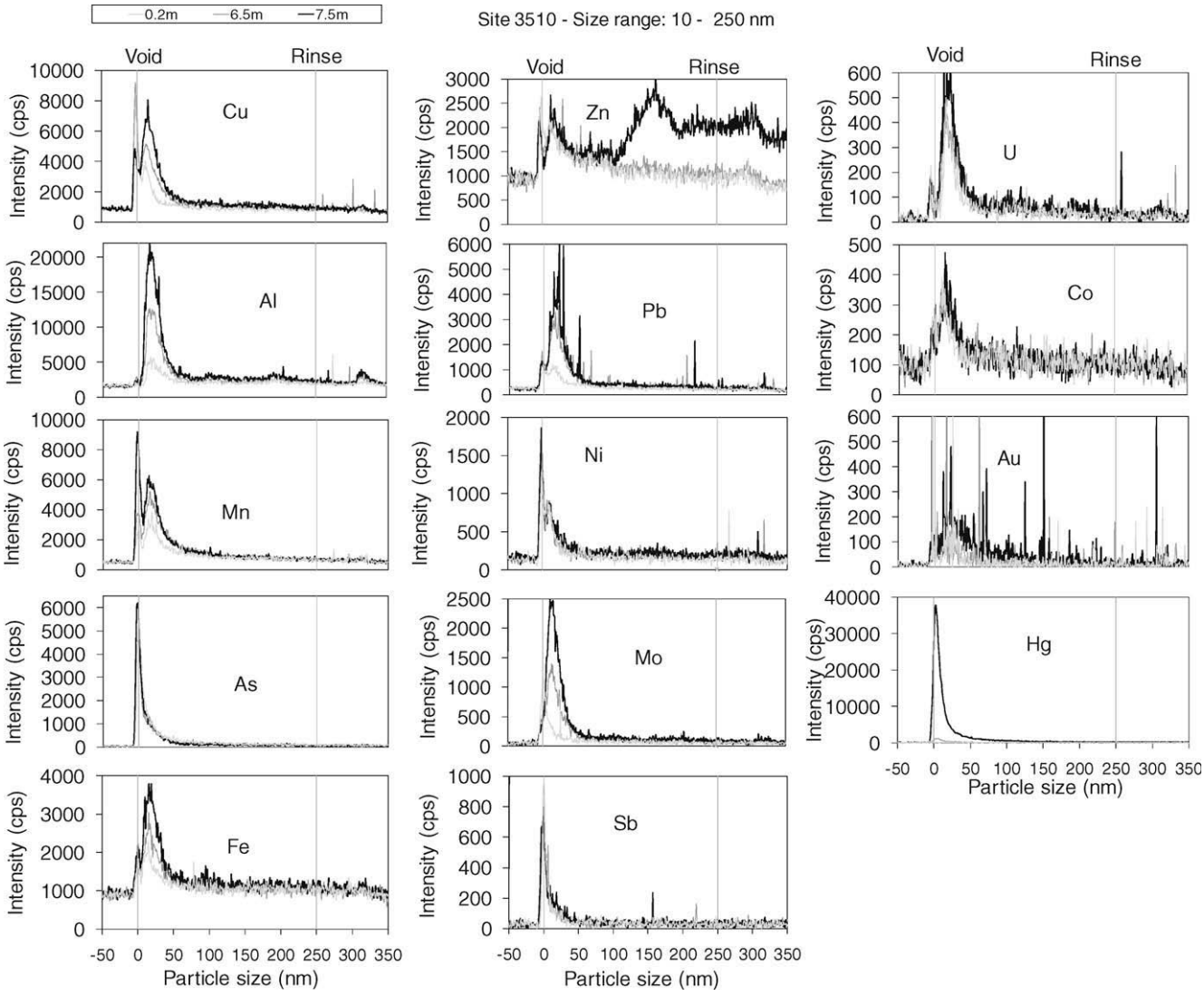

Fig. 5. Fractograms of GSL deep brine sample (site 3510 at 0.2, 6.5 and 7.5 m in depth; samples collected on 10/26/07). Size range: 10–250 nm. These fractograms are representative of the fractograms obtained for the other GSL deep brine sample examined via AF4-CC-ICP-MS.

are not corrected for influences of varied salinity; whereas, these influences are corrected in the integrated elemental masses described below. Nanoparticle sizes reported here correspond to the hydrodynamic diameter of an equivalent sphere (Giddings, 1985, 1993; Beckett et al., 1997; Beckett and Giddings, 1997).

3.2. Trace element concentrations associated with particulates

Fig. 9 shows concentrations (per L solution) of particulate-associated elements as a function of depth and size range. For >450 nm microparticles, the concentrations of nearly all associated elements increased with depth (Fig. 9 top). The same observation held for the 10–250 nm nanoparticles (except Co, As, and Sb) (Fig. 9 middle). In contrast to the >10 nm size range, the majority of the trace element concentrations in the 0.9–7.5 nm size range did not increase with depth (Fig. 9 bottom), except for Al, Mo and Hg.

The majority of trace element mass associated with particulates was in the >450 nm size range, as shown by comparing the measured concentrations (per L solution) between the three particulate size ranges (Fig. 9). The trace element mass associated with the 10–250 nm size range was much lower (multiple orders of magnitude for some elements) relative to the >450 nm size range. The same was true for the 0.9–7.5 nm size range, but with greater concentrations of Ni, Zn, Au and Pb in the 0.9–7.5 nm size range relative to the 10–250 nm size range.

The percent of element mass associated with nano- and microparticulates across the entire size range larger than 0.9 nm (assuming zero losses to the membrane) shows that over 90% of Al, Fe and Mn are associated with >450 nm microparticles at all depths (Fig. 10). Elements such as Co, Cu, Ni and Zn show between 50% and 70% of their mass to be associated with >450 nm microparticles in the shallow brine, whereas this association is about 90% in the deep brine (Fig. 10). In contrast, in the shallow brine, As showed even distribution across the size ranges examined; whereas in the deep brine, around 80% of As in the particulates is in the >450 nm size range (Fig. 10).

The power of AF4-CC-ICP-MS is demonstrated by elements such as Mo, Sb, Pb and U, which were near or below the limit of determination in the shallow brine samples when CC-ICP-MS alone was used. Using AF4-CC-ICP-MS, these elements were observed in nanoparticles in the shallow brine, since these nanoparticles were concentrated via fractionation (Figs. 6 and 8–10).

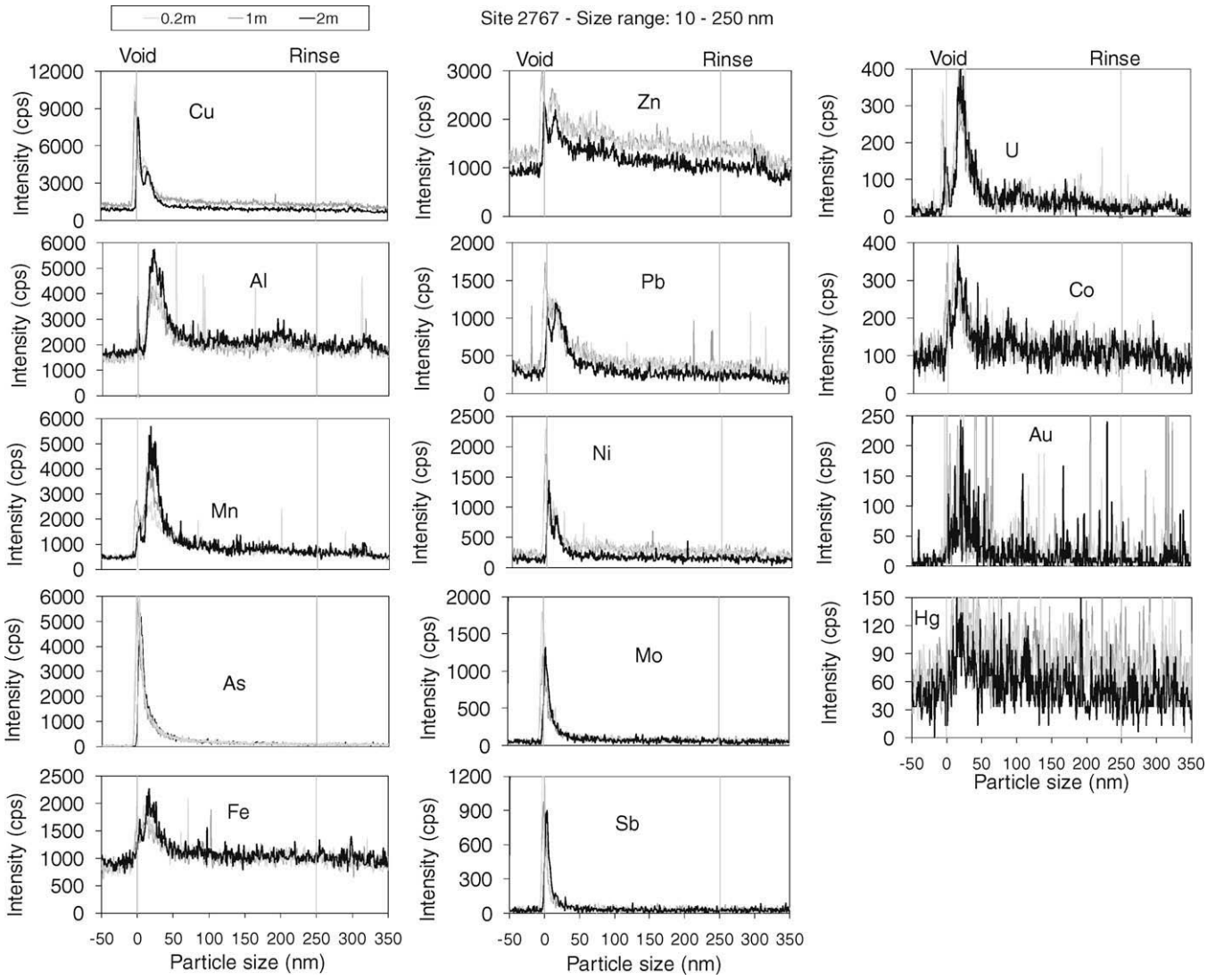

Fig. 6. Fractograms of GSL shallow brine sample (site 2767 at 0.2, 1.0 and 2.0 m in depth; samples collected on 10/25/07). Size range: 10–250 nm. These fractograms are representative of the fractograms obtained for the other GSL shallow brine samples examined via AF4-CC-ICP-MS.

4. Discussion

The dominance of >450 nm particles may be related to aggregate formation due to the salinity and element concentrations in the GSL. Baalousha et al. (2006c) found that larger size aggregates of organic colloids were formed at high salinity, and the high ionic strength of the GSL also supports aggregation (Maximova and Dahl, 2006; Dahlqvist et al., 2004; Wigginton et al., 2007; Stolpe and Hassellöv, 2007; Lead et al., 2000; Benincasa et al., 2002; Siripinyanond et al., 2005; Schmitt et al., 2002). Aggregates may also form through hydrophobic association, charge interactions, H-bonds and metal bridging (Baalousha et al., 2006c). The relatively high density of the GSL brines (1100 kg m^{-3} and 1160 kg m^{-3} for the shallow and deep brines, respectively) relative to most aquatic systems also supports buoyant stabilization of larger colloids. The relative lack of trace element association with colloids in the 100–450 nm size range (except for Zn) may be surprising; however, this finding is not unique to this study. For example, Morrison and Benoit (2004) found that in a fresh water from the Hammonasset River (Connecticut, USA) nearly all Cu was associated with colloids in the size range corresponding to dissolved organic matter, with no Cu association to larger size fractions.

Similarities in size distribution and elemental composition were observed among the shallow and deep brine samples. This was unexpected considering the vastly different geochemical conditions in the two layers (Tayler et al., 1980; Stephens, 1990; Gwynn, 2002), as shown in Figs. 1 and 2. Similarities among particulates in the two geochemically distinct layers could potentially arise from the downward transport of nanoparticles from the shallow to the deep brine layer. However, this is unlikely, since settling times needed are long in these dense aqueous matrices; e.g. the shortest settling time (two months) based on Stoke's settling velocities corresponds to the >450 nm particles (details provided in Supplementary material). Physical mixing between the layers of the GSL is a possibility given that the lake is rarely quiescent (Beisner et al., in press). Disturbance of the lake due to storms and wind events occurs frequently, potentially mixing material between the two layers (Beisner et al., in press). Direct evidence supporting material mixing within the deep layer is provided by sediment trap measurements, which show negligible deposition in shallow traps

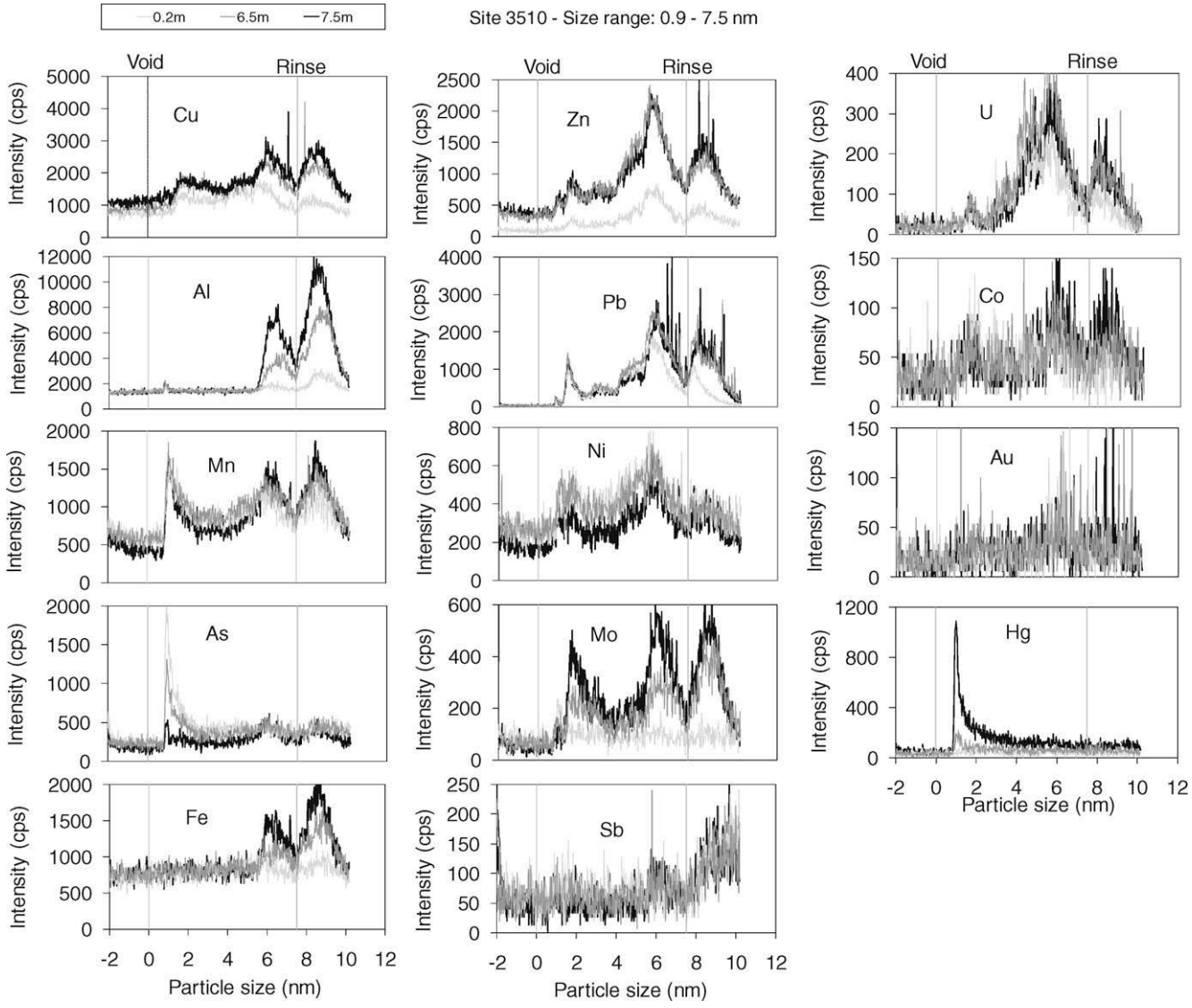

Fig. 7. Fractograms of GSL deep brine water sample (site 3510 at 0.2, 6.5 and 7.5 m in depth; samples collected on 10/26/07). Size range: 0.9–7.5 nm. These fractograms are representative of the fractograms obtained for the other GSL deep brine sample examined via AF4-CC-ICP-MS.

and significant deposition in deep traps, indicating periodic resuspension of bottom sediment (Oliver, 2008). Sediment resuspension is also indicated by the presence of ^{7}Be in sediment core samples (Oliver et al., 2009). The above observations indicate limited material mixing at depth, but the degree of mixing between the shallow and deep brine layers requires further investigation, and at this time it is not possible to know whether mixing events may help to explain the similarity in size distribution and composition of nanomaterials between the two layers.

The observation of similar nanoparticle size distributions in the two distinct brine layers may potentially indicate that the observed distributions do not reflect *in-situ* distributions. Disaggregation of colloids during AF4 fractionation may occur due to dilution in the carrier solution (Buffle and Leppard, 1995), which had an ionic strength (0.01 M NaCl and approx. 10^{-3} M FL-70) (Koliadima and Karaiskakis, 1994) more than two orders of magnitude lower than the hypersaline samples (2.5 M for the shallow). This reduction in solution ionic strength during analysis might potentially allow weak aggregates to break apart via increased mutual electrostatic repulsion (Baalousha et al., 2006c; Bolea et al., 2006; Reynolds, 2005; Li et al., 2008). It should be noted that surfactant was not present in the carrier solution for the 0.9–7.5 nm size fractions. Although it seems unlikely that disaggregation would yield equivalent size distributions from the two distinct brine samples, the possibility of disaggregation exists. For freshwater samples, the concern is usually for aggregation during the focusing step due to elevated carrier ionic strength relative to the sample, as well as near-membrane accumulation (Wigginton et al., 2007; Buffle and Leppard, 1995; Lyvén et al., 2003). In this study, spiking of GSL samples with PSS (8 kDa, 18 kDa, 35 kDa, 100 kDa) yielded signal intensities and elution times that were expected from these standards, indicating that no unexpected influences on spiked primary particle fractionation arose from injection of the brine samples. The relationship of observed versus *in-situ* nanoparticle size distributions requires further investigation via variation of carrier ionic strength up to hypersaline, which is a difficult process that potentially risks the integrity of both the AF4 and the CC-ICP-MS.

It is also possible that the observed nanoparticle size distributions represent *in-situ* size distributions. Several studies have observed bi-modal size distributions in the 1–10 nm size range (Lyvén et al., 2003; Hassellöv et al., 1999; Dahlqvist et al., 2004; Stolpe et al., 2005; Andersson et al., 2006; Stolpe and Hassellöv,

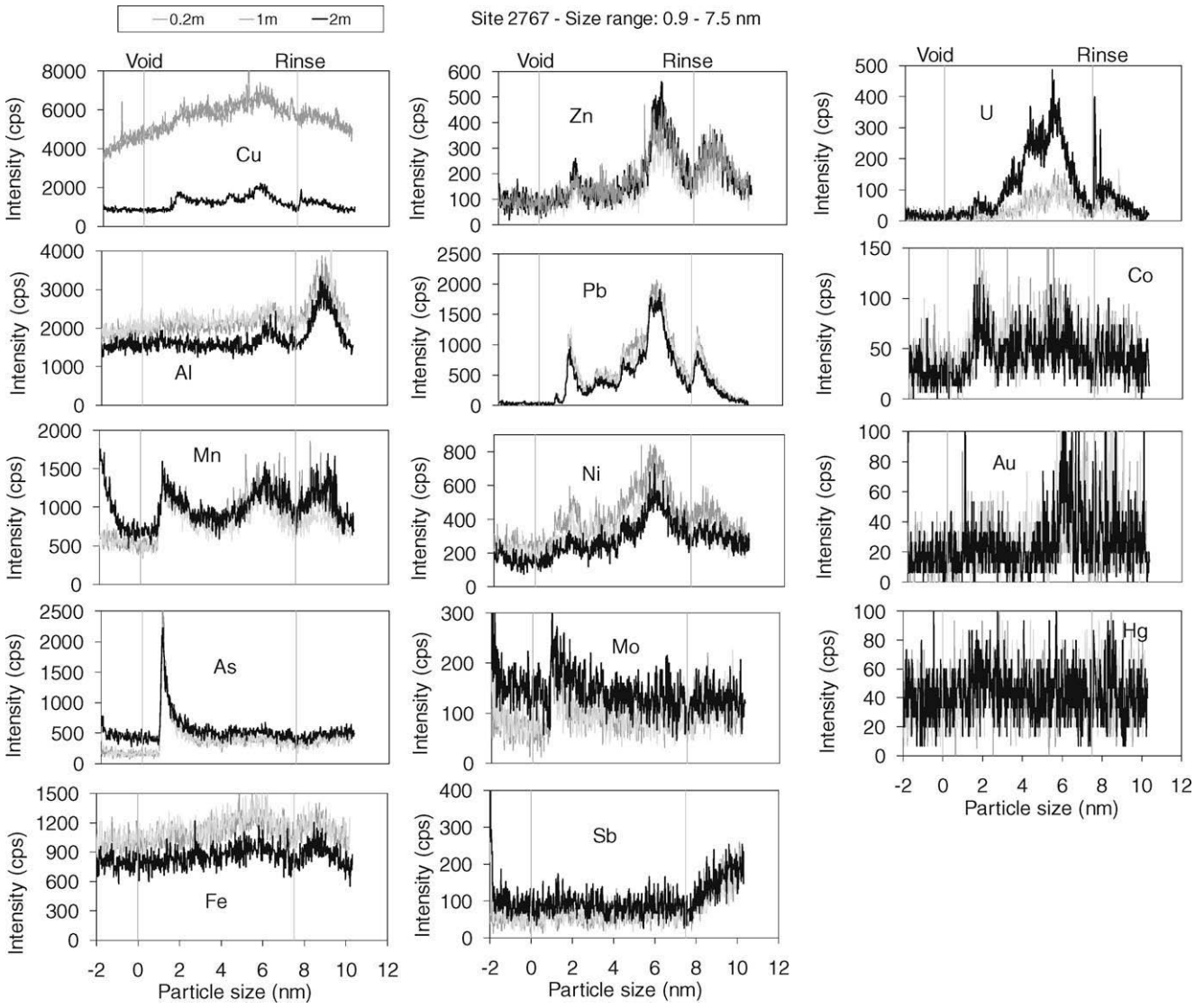

Fig. 8. Fractograms of GSL shallow brine sample (site 2767 at 0.2, 1.0 and 2.0 m in depth; samples collected on 10/25/07). Size range: 0.9–7.5 nm. These fractograms are representative of the fractograms obtained for the other GSL shallow brine samples examined via AF4-CC-ICP-MS.

2007) attributing the smaller size fraction to association with NOM, and the larger size fraction to association with minerals (typically Fe oxides since most studies were performed in oxic waters). In the present results, trace metals such as Mn, Ni, Co, Pb, Cu, Zn and Mo were associated with 1–3-nm nanoparticles (Figs. 7 and 8), which are attributed to sulfides for Pb, Cu, Zn and Mo due to their increased concentrations with depth (degree of anoxia). However, it is also possible that this small size fraction is associated with organic C, which also increased in concentration with depth, from a minimum of 20.4 mg TOC/L to a maximum of 138.7 mg TOC/L in the shallow to deep brine transition.

For elements such as Fe in the nominally-dissolved size fraction (e.g. <200 nm), between 40% and 96% of nominally dissolved mass has been demonstrated to be associated with nanoparticles (Sañudo-Wilhelmy et al., 1996; Wen et al., 1999; Wells et al., 2000). The present study also shows this result (Fig. 11), where 38% of nominally-dissolved (<450 nm size fraction) Fe mass was associated with nanoparticles. The truly dissolved fraction was determined by difference between the <450 nm fraction and the summed nanoparticle fractions (0.9–7.5 nm plus 10–250 nm). Notably, Zn and Cu showed 10% and 14%, respectively, of their nominally-dissolved mass associated with nanoparticles. All other elements showed negligible percent mass associated with nanoparticles in the nominally-dissolved fraction.

SEM – EDX analysis of >450 nm particles from the shallow and deep brine samples showed an abundance of clays in both the shallow oxic and deep anoxic samples (Figs. 12 and 13). These phases were predicted via approximate speciation simulations using the geochemical equilibrium speciation program PHREEQC (details in Supplementary material) and may help to explain the elemental composition similarities found in the results from the oxic and anoxic brines. Sulfur was detected only in the deep brine samples

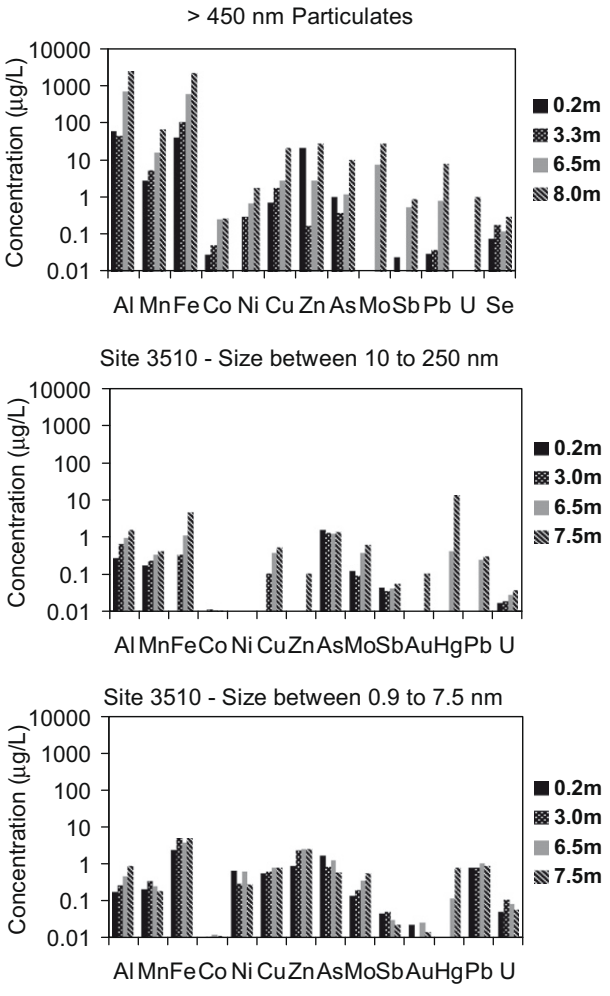

Fig. 9. Concentration of trace elements for site 3510 at 0.2 m, 3.0, 6.5 and 7.5 m in depth. Top: size range >450 nm. Middle: size range between 10 and 250 nm. Bottom: size range between 0.9 and 7.5 nm.

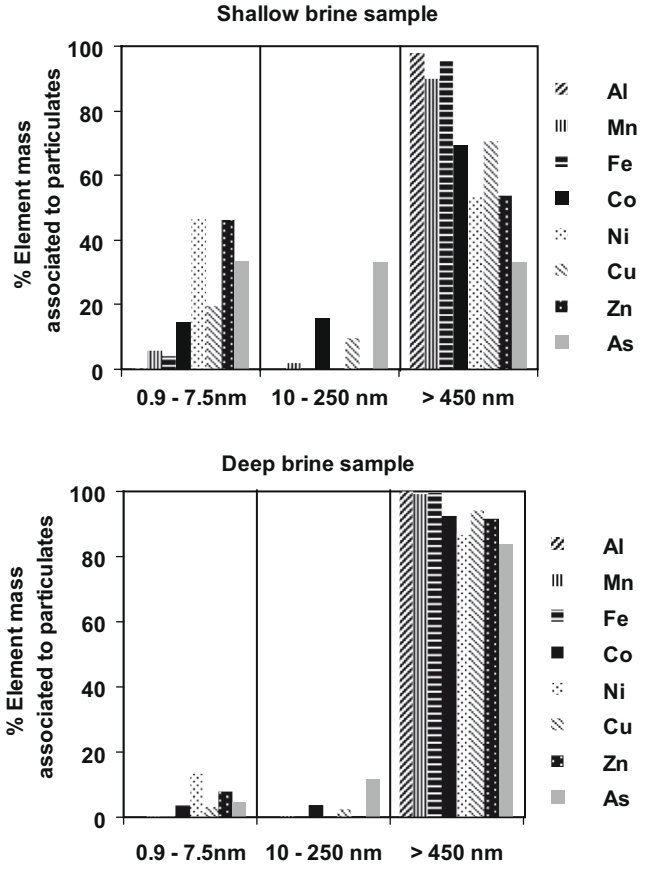

Fig. 10. Distribution of particulate-associated trace elements among three size ranges. Results for shallow brine layer sample (top) and deep brine layer sample (bottom). Sum of percent across all three size ranges equals 100.

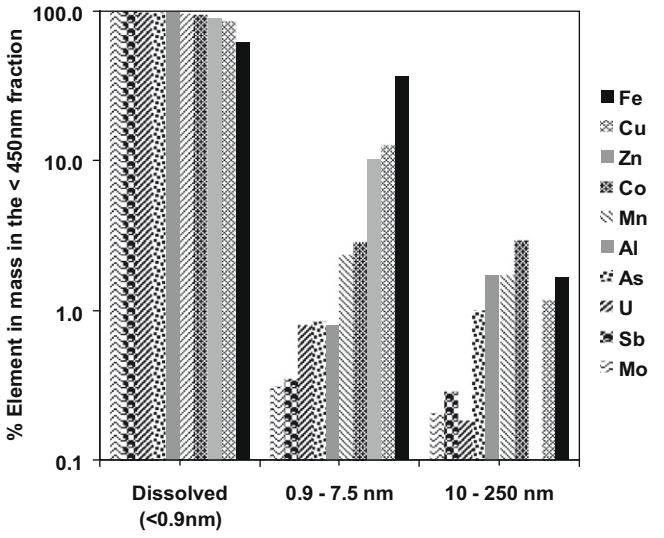

Fig. 11. Average distribution (in percentage) of trace elements in nanoparticles in the <450 nm fraction. Site 3510, shallow brine samples.

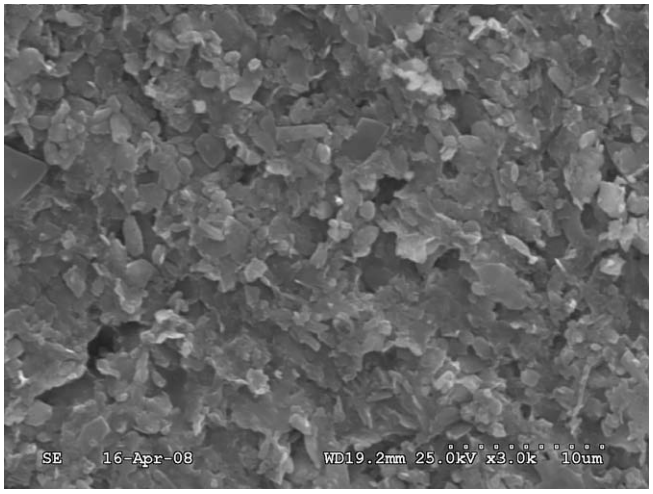

Fig. 12. SME–EDX results from a raw unacidified (RU) deep sample collected at site 2565, showing agglomerated particles formed mainly of clays.

(Fig. 13 bottom), suggesting the presence of sulfides, which were also predicted by PHREEQC to occur solely in the deep brine. This expectation corroborates the nanoparticle fractograms (Figs. 5 and 7) showing strong increases with depth in signal intensities for elements that are expected to form sulfide minerals (e.g. Mo, Zn, Cu, Pb). Arsenic would also be expected to associate with sulfide; however, its concentration (in the <7.5 nm fraction) was much greater in the oxic shallow brine relative to the anoxic deep brine, possibly due to the formation of arsenite, which is a highly stable dissolved species under reduced conditions (Drever, 2002). Mercury in the anoxic deep brine might also be expected to associate with sulfide nanoparticles; however, Figs. 5 and 7 indicate association with molecular-scale moieties; e.g. dissolved organic matter macromolecules.

Trace element concentration measurements made over an annual period showed different trends depending on the element, with elements such as Al, Fe and Mn showing much greater temporal variability relative to the other elements (Figs. S7 and S8 in Supplementary material). In the shallow brine, Al and Fe showed large increases in particulate mass (defined as the difference between the raw acidified and the filtered acidified samples) during the fall-winter season; whereas, Mn showed increases in dissolved mass only. These results suggest that Fe and Al are associated with one another in >450 nm particulates in the shallow brine layer. Aluminium, Fe and Mn were also notably variable in the deep brine

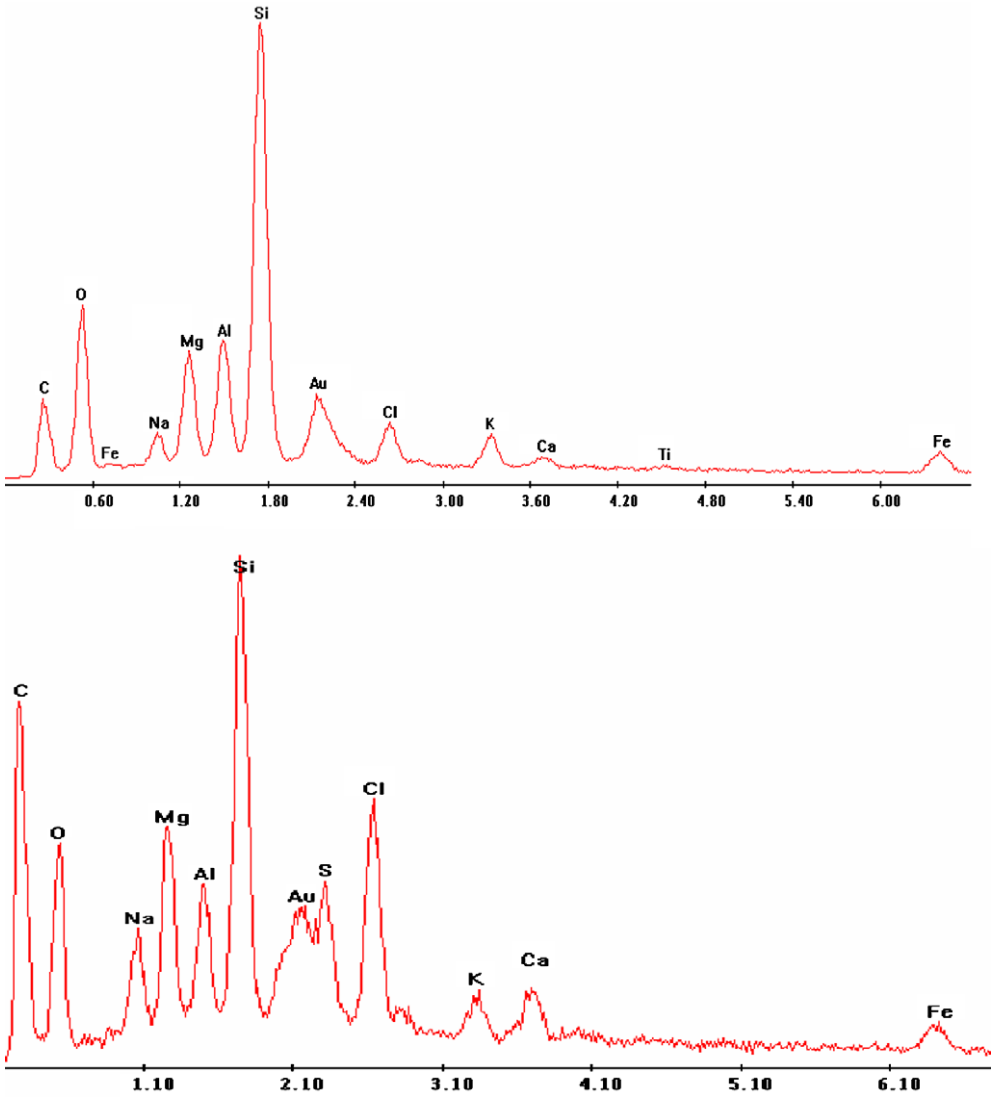

Fig. 13. SME–EDX results from raw unacidified (RU) samples. Top: shallow sample collected at site 2267 at 2.5 m in depth. Bottom: deep sample collected at site 2565 at 7.5 m in depth.

layer, where all three showed increased concentrations in particulates in November, April and May, strongly suggesting their mutual association in >450 nm particulates in the deep brine layer. Although the cause of these different behaviors is not known, the differences in the temporal variability of these elements in the shallow and deep brine layers are consistent with the expectations of different mineralogical assemblages among the two layers. Given the lack of means to estimate activity coefficients for these elements under hyper-saline conditions, it is not possible to provide a rigorous geochemical speciation explanation for the observed seasonal trends and elemental associations. However, it is reasonable to expect them to be driven by seasonal variations in concentration and dilution (lake volume, Baskin, 2005), temperature, dissolved O_2, pH, etc., as shown in Figs. 1 and 2.

5. Conclusions

This work determined the size distribution and chemical composition of micro and nanoparticulates from the geochemical stratified layers of the water column of the GSL. For the majority of, the trace elements concentrations were higher in the anoxic deep brines than in the oxic shallow brines, for all size ranges (0.9–7.5 nm, 10–250 nm, >450 nm). Trace elements in the GSL were found mainly associated with >450 nm particles, over 90% of Al, Fe and Mn mass, and over 55% of Co, Cu, Ni, and Zn mass were associated with these particles. The stability of these large particles results from aggregation and buoyancy in this hypersaline environment.

The apparent similar nanoparticle size distribution between the two layers contrasts with the differences in nanoparticle chemical composition between the brine layers, which include the presence of detectable S only in the deep (anoxic) brine layer, and differences in temporal trends in particulate-associated elements. Additional research will be needed to understand the degree to which the observed nanoparticle size distributions reflect *in-situ* size distributions.

Differences in elemental associations to nanoparticles were discerned; e.g. elements such as Zn, Cu, Pb and Mo were associated with two sizes of nanoparticles (approximately 2 and 6 nm) and showed increasing concentrations with depth (degree of anoxia) suggesting the formation of sulfide nanoparticles, although it is possible that the smaller of the bi-modal size fractions reflects association with dissolved organic matter, which also increases with depth. Elements such as Mn, Ni and Co, were associated with nanoparticulates in the ca. 2-nm and 6-nm sizes; however, their signal intensities were nearly equivalent in the deep and shallow brine layers. Elements such as Al and Fe showed greatly increased concentration with depth; however, they were associated only with ~6 nm colloids, possibly reflecting association with clays rather than sulfides. Uranium was associated with 4–6 nm nanoparticles with no change in concentration with depth. Arsenic was associated with <2 nm nanoparticles, and showed no increase in concentration with depth, possibly indicating dissolved arsenite. Mercury was associated with <2 nm nanoparticles, and showed greatly increased concentration with depth, possibly indicating association with dissolved organic matter.

Acknowledgments

This project was funded by the State of Utah – Department of Environmental Quality – Division of Water Quality (DWQ) and the US Geological Survey (USGS). Use of brand names in this publication does not constitute endorsement by either the University of Utah or the US Geological Survey. The authors want to thank Dr. Ronald Beckett and the anonymous reviewer for the helpful comments during review of this manuscript.

Appendix A. Supplementary material

Supplementary data associated with this article can be found, in the online version, at doi:10.1016/j.apgeochem.2009.04.031.

References

Al-Ammar, A., Siripinyanond, A., Barnes, R.M., 2001. Simultaneous sample preconcentration and matrix removal using field-flow fractionation coupled to inductively coupled plasma mass spectrometry. Spectrochim. Acta Part B 56, 1951–1962.

Aldrich, T.W., Paul, D.S., 2002. Avian ecology of Great Salt Lake. In: Gwynn, J.W. (Ed.), Great Salt Lake: An Overview of Change. Utah Department of Natural Resources Special Publication, Salt Lake City, pp. 43–374.

Amarasiriwardena, D., Siripinyanond, A., Barnes, R.M., 2001. Trace elemental distribution in soil and compost-derived humic acid molecular fractions and colloidal organic matter in municipal wastewater by flow field-flow fractionation-inductively coupled plasma mass spectrometry (flow FFF-ICP-MS). J. Anal. Atom. Spectrom. 16, 978–986.

Andersson, K., Dahlqvist, R., Turner, D., Stolpe, B., Larsson, T., Ingri, J., Andersson, P., 2006. Colloidal rare earth elements in a boreal river: Changing sources and distributions during the spring flood. Geochim. Cosmochim. Acta 70, 3261–3274.

Baalousha, M., Lead, J.R., 2007a. Characterization of natural aquatic colloids (<5 nm) by flow-field flow fractionation and atomic force microscopy. Environ. Sci. Technol. 41, 1111–1117.

Baalousha, M., Lead, J.R., 2007b. Size fractionation and characterization of natural aquatic colloids and nanoparticles. Sci. Total Environ. 386, 93–102.

Baalousha, M., Kammer, F.V.D., Motelica-Heino, M., Baborowski, M., Hofmeister, C., Le Coustumer, P., 2006a. Size-based speciation of natural colloidal particles by flow field flow fractionation, inductively coupled plasma-mass spectroscopy, and transmission electro microscopy/X-ray energy dispersive spectroscopy: colloids – trace element interaction. Environ. Sci. Technol. 40, 2156–2162.

Baalousha, M., Kammer, F.V.D., Motelica-Heino, M., Hilal, H.S., Le Coustumer, P., 2006b. Size fractionation and characterization of natural colloids by flow-field flow fractionation coupled to multi-angle laser light scattering. J. Chromatogr. A. 1104, 272–281.

Baalousha, M., Motelica-Heino, M., Le Coustumer, P., 2006c. Conformation and size of humic substances: Effects of major cation concentration and type, pH, salinity, and residence time. Colloids Surf. A: Physicochem. Eng. Aspects 272, 48–55.

Barman, B.N., Moon, M.E., 2000. Sample preparation and choice of carrier liquid in field-flow fractionation. In: Schimpf, M.E., Caldwell, K., Giddings, J.C. (Eds.), Field Flow Fractionation Handbook. Wiley-Interscience Inc., New York, pp. 89–198.

Baskin, R.L., 2005. Calculation of area and volume for the south part of the Great Salt Lake, Utah. US Department of Interior, US Geol. Surv. Open-File Report 2005-1327.

Beckett, R., 1991. Field-flow fractionation-ICP-MS: a powerful new analytical tool for characterizing macromolecules and particles. Atom. Spectrosc. 12, 228–232.

Beckett, T., Giddings, C., 1997. Entropic contribution to the retention of nonspherical particles in field-flow fractionation. J. Colloid Interf. Sci. 186, 53–59.

Beckett, R., Hart, B.T., 1993. Use of field-flow fractionation techniques to characterize aquatic particles, colloids, and macromolecules. In: Buffle, J., van Leeuwen, H.P. (Eds.), Environmental Particles, Vol. 2. Lewis, Publishers, Chelsea, p. 993.

Beckett, R., Murphy, D., Tadjiki, S., Chittleborough, D.J., Giddings, J.C., 1997. Determination of thickness, aspect ratio and size distributions for platey particles using sedimentation field-flow fractionation and electron microscopy. Colloid Surf. Physicochem. Eng. Aspect 120, 17–26.

Beisner, K., Naftz, D.L., Johnson, W.P., Diaz, X., in press. Selenium and trace element mobility affected by periodic displacement of stratification in the Great Salt Lake, Utah. Sci. Total Environ.

Benincasa, M.A., Caroni, G., Imperia, N., 2002. Effect of ionic strength and electrolyte composition on the aggregation of fractionated humic substances studied by flow field-flow fractionation. J. Separat. Sci. 25, 405–415.

Bolea, E., Gorriz, M.P., Bouby, M., Laborda, F., Castillo, J.R., Geckeis, H., 2006. Multielement characterization of metal-humic substances complexation by size exclusion chromatography, asymmetrical flow field-flow fractionation, ultrafiltration and inductively coupled plasma-mass spectrometry detection: a comparative approach. J. Chromatogr. A 1129, 236–246.

Buffle, J., Leeuwen, H. (Eds.), 1992. Environmental Particles I. CRC press, Boca Raton, FL.

Buffle, J., Leeuwen, H.P.V. (Eds.), 1993. Environmental Particles II. CRC press, Boca Raton, FL.

Buffle, J., Leppard, G.G., 1995. Characterization of aquatic colloids and macromolecules. 1. Structure and behavior of colloidal material. Environ. Sci. Technol. 29, 2169–2175.

Cardot, P.J.P., Rasouli, S., Blanchart, P., 2001. TiO_2 colloidal suspension polydispersity analysed with sedimentation field flow fractionation and electron microscopy. J. Chromatogr. A 905, 163–173.

Chen, Z.L., Khana, N.I., Owensa, G., Naidu, R., 2007. Elimination of chloride interference on arsenic speciation in ion chromatography inductively coupled mass spectrometry using an octopole collision/reaction system. Microchem. J. 87, 87–90.

Cho, J., Kim, I.S., Moon, J., Kwon, B., 2006. Determining Brownian and shear-induced diffusivity of nano- and micro-particles for sustainable membrane filtration. Desalination 188, 213–216.

Contado, C., Blo, G., Conato, C., Dondi, F., Beckett, R., 2003. Experimental approaches for size-based metal speciation in rivers. J. Environ. Monit. 5, 845–851.

Dahlqvist, R., Benedetti, M.F., Andersson, K., Turner, D., Larsson, T., Stolpe, B., Ingri, J., 2004. Association of calcium with colloidal particles and speciation of calcium in the Kalix and Amazon rivers. Geochim. Cosmochim. Acta 68, 4059–4075.

Dai, M.H., Martin, J.M., 1995. First data on trace metal level and behaviour in two major Arctic river-estuarine systems (Ob and Yenisey) and in the adjacent Kara Sea, Russia. Earth Planet Sci. Lett. 131, 127–141.

Dobbeleir, J., Adam, N., Bossuyt, E., Bruggeman, E., Sorgeloos, P., 1980. New aspects of the use of inert diets for high density culturing of brine shrimp. In: Sorgeloos, P., Bengtson, D., Decleir, W., Jaspers, E. (Eds.), The Brine Shrimp Artemia. Ecology, Culturing, Use in Aquaculture, Vol. 3. Universa Press, Wetteren, Belgium, pp. 65–174.

Drever, J.I., 2002. The Geochemistry of natural waters, surface and groundwater environments, 3rd ed. Reprinted. Prentice Hall, Upper Saddle River.

Giddings, J.C., 1985. Field-flow fractionation. Separat. Sci Technol. 19, 831–847.

Giddings, J.C., 1993. Field-flow fractionation: analysis of macromolecular, colloidal and particulate materials. Science 260, 1456–1465.

Gilbert, B., Lu, G., Kim, C.S., 2007. Stable cluster formation in aqueous suspensions of iron oxyhydroxide nanoparticles. J. Colloid Interf Sci. 313, 152–159.

Gwynn, J.W., 2002. Great Salt Lake, Utah: chemical and physical variation of the brine and effects of the SPRR causeway, 1966–1996. In: Gwynn, J.W. (Ed.), Great Salt Lake: An Overview of Change. Utah Department of Natural Resources Special Publication, pp. 87–106.

Hassellöv, M., Lyvén, B., Haraldsson, C., Sirinawin, W., 1999. Determination of continuous size and trace element distribution of colloidal material in natural water by on-line coupling of flow field-flow fractionation with ICPMS. Anal. Chem. 71, 3497–3502.

Hillwalker, W.E., 2004. Selenium and trace metal accumulation in detrital-benthic food webs of lotic and lentic wetlands, Utah, USA. Ph.D. Dissertation, Oregon State Univ., Corvallis, USA.

Hochella Jr., M.F., Lower, S.K., Maurice, P.A., Penn, R.L., Sahai, N., Sparks, D.L., Twining, B.S., 2008. Nanominerals, mineral nanoparticles, and earth systems. Science 319, 1631–1635.

Jarvie, H.P., King, S.M., 2007. Small-angle neutron scattering study of natural aquatic nanocolloids. Environ. Sci. Technol. 41, 2868–2873.

Jeon, S.J., Schimpf, M.E., Nyborg, A., 1997. Compositional effects in the retention of colloids by thermal field-flow fractionation. Anal. Chem. 69, 3442–3450.

Koliadima, A., Karaiskakis, G., 1994. Concentration and characterization of dilute colloidal samples by potential-barrier field-flow fractionation. Chromatographia 39, 74–78.

Kraepiel, A.M.L., Chiffoleau, J.F., Martin, J.M., Morel, F.M.M., 1997. Geochemistry of trace metals in the Gironde estuary. Geochim. Cosmochim. Acta 61, 1421–1436.

Lead, J.R., Wilkinson, K.J., 2006. Environmental colloids and particles: Current knowledge and future developments. In: Lead, J.R., Wilkinson, K.J. (Eds.), Environmental Colloids and Particles: Behaviour, Separation and Characterisation. John Wiley and Sons, Chichester, UK.

Lead, J.R., Wilkinson, K.J., Balnois, E., Cutak, B.J., Larive, C.K., Assemi, S., Beckett, R., 2000. Diffusion coefficients and polydispersities of the Suwannee River fulvic acid: comparison of fluorescence correlation spectroscopy, pulsed-field gradient nuclear magnetic resonance, and flow field-flow fractionation. Environ. Sci. Technol. 34, 3508–3513.

Li, Q., Jonas, U., Zhao, X.S., Kapp, M., 2008. The forces at work in colloidal self-assembly: a review on fundamental interactions between colloidal particles. Asia-Pacific J. Chem. Eng. 3, 255–268.

Lin, A., 1976. A survey of physical limnology of Great Salt Lake, Utah. Division of Water Resources – Comprehensive Water Planning Program.

Lyvén, B., Hassellov, M., Turner, D.R., Haraldsson, C., Anderson, K., 2003. Competition between iron- and carbon-based colloidal carriers for trace metals in a freshwater assessed using flow field-flow fractionation coupled to ICPMS. Geochim. Cosmochim. Acta 67, 3791–3802.

Maximova, N., Dahl, O., 2006. Environmental implications of aggregation phenomena: Current understanding. Curr. Opin. Colloid Interf. Sci. 11, 246–266.

McCarthy, J.E., Zachara, J.M., 1989. Subsurface transport contaminants. Environ. Sci. Technol. 23, 496–502.

Moon, M.H., 1995. Effect of carrier solutions on particle retention in flow field-flow fractionation. Bull. Korean Chem. Soc. 16, 613–619.

Morrison, M.A., Benoit, G., 2001. Filtration artifacts caused by overloading membrane filters. Environ. Sci. Technol. 35, 3774–3779.

Morrison, M.A., Benoit, G., 2004. Investigation of conventional membrane and tangential flow ultrafiltration artifacts and their application to the characterization of freshwater colloids. Environ. Sci. Technol. 38, 6817–6823.

Murphy, D.M., Gabarino, J.R., Taylor, H.E., Hart, B.T., Beckett, R., 1993. Determination of size and element composition distribution of complex colloids by sedimentation field-flow fractionation inductively coupled plasma mass spectrometry. J. Chromatog. 642, 459–467.

Naftz, D.L., Angeroth, C., Kenney, T., Waddell, B., Darnall, N., Silva, S., Perschon, C., Withehead, J., 2008. Anthropogenic influences on the input and biogeochemical cycling of nutrients and mercury in Great Salt Lake, Utah, USA. Appl. Geochem. 23, 1731–1744.

Oliver W.A., 2008. Selenium removal processes from Great Salt Lake, Utah: estimating sedimentation and verifying volatilization fluxes. Unpublished MS. Thesis, Univ. Utah, Salt Lake City.

Oliver, W., Fuller, C., Naftz, D.L., Johnson, W.P., Diaz, X., 2009. Estimating selenium removal by sedimentation from the Great Salt Lake, Utah. Appl. Geochem. 24, 936–949.

Prestel, H., Schott, L., Niessner, R., Panne, U., 2005. Characterization of sewage plant hydrocolloids using asymmetrical flow field-flow fractionation and ICP-mass spectrometry. Water Res. 39, 3541–3552.

Prestel, H., Niessner, R., Panne, U., 2006. Increasing the sensitivity of asymmetrical flow field-flow fractionation: slot outlet technique. Anal. Chem. 78, 6664–6669.

Ranville, J.F., Chittleborough, D.J., Shanks, F., Morrison, R.J.S., Harris, T., Doss, F., Beckett, R., 1999. Development of sedimentation field-flow fractionation-inductively coupled plasma mass spectrometry for the characterization of environmental colloids. Anal. Chim. Acta 381, 315–329.

Ranville, J.F., Hendry, M.J., Reszat, T.N., Xie, Q., Honeyman, B.D., 2007. Quantifying uranium complexation by groundwater dissolved organic carbon using asymmetrical flow field-flow fractionation. J. Contam. Hydrol. 91, 233–246.

Reschiglian, P., Melucci, D., Zattoni, A., Mallo, A., Hansen, M., Kummerow, A., Miller, M., 2000. Working without accumulation membrane in flow field-flow fractionation. Anal. Chem. 72, 5945–5954.

Reynolds, C.S., 2005. Physical properties of water relevant to limnology and limnetic ecology. In: O'Sullivan, P.E., Reynolds, C.S. (Eds.), The Lakes Handbook: Limnology and Limnetic Ecology, Vol. 1. Blackwell Publishing, Malden, pp. 07–114.

Sañudo-Wilhelmy, S.A., Rivera-Duarte, I., Flegal, A.R., 1996. Distribution of colloidal trace metals in the San Francisco Bay estuary. Geochim. Cosmochim. Acta 60, 4933–4944.

Schmitt, D., Taylor, H.E., Aiken, G.R., Roth, D.A., Frimmel, F.H., 2002. Influence of natural organic matter on the adsorption of metal ions onto clay minerals. Environ. Sci. Technol. 36, 2932–2938.

Singhal, R.K., Preetha, J., Karpe, R., Tirumlesh, K., Kumar, S.C., Hegde, A.G., 2006. The use of ultrafiltration in trace metal speciation studies in sea water. Environ. Int. 32, 224–228.

Siripinyanond, A., Barnes, R.M., Amarasiriwardena, D., 2002. Field flow fractionation-inductively coupled plasma mass spectrometry for sediment bound trace metal characterization. J. Anal. Atom. Spectrom. 17, 1055–1064.

Siripinyanond, A., Worapanyanond, S., Shiowatana, J., 2005. Field-flow fractionation–inductively coupled plasma mass spectrometry: an alternative approach to investigate metal–humic substances interaction. Environ. Sci. Technol. 39, 3295–3301.

Stephens, D.W., 1990. Change in lake levels, salinity and the biological community of Great Salt Lake (Utah, USA), 1847–1987. Hydrobiologia 19, 139–146.

Stolpe, B., Hassellöv, M., 2007. Changes in size distribution of fresh water nanoscale colloidal matter and associated elements on mixing with seawater. Geochim. Cosmochim. Acta 71, 3292–3301.

Stolpe, B., Hassellöv, M., Andersson, K., Turner, D.R., 2005. High resolution ICPMS as an on-line detector for flow field flow fractionation; multi-element determination of colloidal size distributions in a natural water sample. Anal. Chim. Acta 535, 109–121.

Suteerapataranon, S., Bouby, M., Geckeis, H., Fanghänel, T., Grudpan, K., 2006. Interaction of trace elements in acid mine drainage solution with humic acid. Water Res. 40, 2044–2054.

Tayler, P.I., Hutchinson, L.A., Muir, M.K., 1980. Heavy metals in the Great Salt Lake, Utah. In: Gwynn, J.W. (Ed.), Great Salt Lake a Scientific, Historical and Economic Overview, vol. 116. Utah Geological and Minerals Survey, Salt Lake City, Bull., pp. 95–199.

Taylor, H.E., 2001. Inductively Coupled Plasma-Mass Spectrometry: Practices and Techniques. Academic Press, San Diego.

Taylor, H.E., Garbarino, J.R., Murphy, D.M., Beckett, R., 1992. Inductively coupled plasma-mass spectrometry as an element specific detector for field-flow fractionation particle separation. Anal. Chem. 64, 2036–2041.

Wahlund, K.-G., 2000. Asymmetrical flow field-flow fractionation. In: Schimpf, M.E., Caldwell, K., Giddings, J.C. (Eds.), Field Flow Fractionation Handbook. Wiley-Interscience Inc., New York, pp. 79–294.

Wells, M.L., Kozelka, P.B., Bruland, K.W., 1998. The complexation of 'dissolved' Cu, Zn, Cd and Pb by soluble and colloidal organic matter in Narragansett Bay, RI. Mar. Chem. 62, 203–217.

Wells, M.L., Smith, G.J., Bruland, K.W., 2000. The distribution of colloidal and particulate bioactive metals in Narragansett Bay, RI. Marine Chem. 71, 143–163.

Wen, L.S., Santschi, P.H., Gill, G.A., Paternostro, C.L., Lehman, R.D., 1997. Colloidal and particulate silver in river and estuarine waters of Texas. Environ. Sci. Technol. 31, 723–731.

Wen, L-S., Santschi, P., Gill, G., Paternostro, C., 1999. Estuarine trace metal distribution in Galveston Bay: importance of colloidal forms in the speciation of the dissolved phase. Marine Chem. 63, 185–212.

Wigginton, N.S., Haus, K.L., Hochella, M.F. Jr., 2007. Aquatic environmental nanoparticles. J. Environ. Monit. 9, 1285–1432.

Wurstbaugh, W.A., 1992. Food-web modification by an invertebrate predator in the Great Salt Lake (USA). Oecologia 89, 168–175.